Polymer Journal, Vol. 31, No. 11-2, pp 989—994 (1999)

A Study of Three-Phase Structures in ABC Triblock Copolymers

Yoshihito TANAKA, Hirokazu HASEGAWA,† Takeji HASHIMOTO, Alexander RIBBE, Kenji SUGIYAMA,* Akira HIRAO,* and Seiichi NAKAHAMA*

Department of Polymer Chemistry, Graduate School of Engineering, Kyoto University
Yoshida-honmachi, Sakyo-ku, Kyoto 606-8501, Japan
**Department of Polymer Chemistry, Tokyo Institute of Technology,*
2-12-1 Ohokayama, Meguro-ku, Tokyo 152-8552, Japan

(Received February 16, 1999)

ABSTRACT: The microdomain structure of an ABC triblock copolymer consisting of poly(2-hydroxyethyl methacrylate), poly(*tert*-butyl methacrylate) and poly(2-(perfluorobutyl) ethyl methacrylate) was investigated by means of small-angle X-ray scattering (SAXS) and energy-filtered transmission electron microscopy (EF-TEM) which is based on inelastically scattered electrons by a specific element (F atoms in this case) and known as element spectroscopic imaging (ESI). A three-phase lamellar structure was observed with good contrast for an unstained ultrathin section of the as-cast film of the triblock copolymer by imaging the inelastically scattered electrons at energy-loss of 100 eV. The microdomain structure can be interpreted in accordance with the EF-TEM result. A peculiar SAXS profile where the intensity of the first-order peak was weaker than that of the second-order was observed for the triblock copolymer. Theoretical calculation of the SAXS intensity with a paracrystal model of the four-layer lamellae successfully reproduced the observed SAXS profile.

KEY WORDS ABC Triblock Copolymer / Microphase Separation / Transmission Electron Microscopy / Small-Angle X-Ray Scattering / Element Spectroscopic Imaging

It is well known that an AB diblock copolymer composed of an immiscible polymer pair, A and B, undergoes microphase separation and produces a highly regular periodic structure of A and B microphases with a crystallographic symmetry. Such structures, either in equilibrium or non-equilibrium, have been studied by numerous investigators by means of small-angle X-ray (or neutron) scattering and/or transmission electron microscopy of ultrathin sections. A variety of microdomain morphologies have been reported, e.g., alternating lamellae, hexagonally-packed cylinders, spheres packed in a body-centered cubic lattice, bicontinuous structures (double diamond and double gyroid), and perforated lamellae (or mesh).[1,2]

An ABC triblock copolymer consisting of mutually immiscible A, B and C polymeric sequence also undergoes microphase separation to form three independent microphases. Three-phase microdomain structures of ABC triblock copolymers have been systematically studied by several research groups.[3–6] However, recent developments in experimental[7] and theoretical[8,9] studies revealed tremendous complexity in the microphase separation of ABC triblock copolymers. An addition of C block to an AB diblock copolymer introduces new problems in the thermodynamics and kinetics of the phase transition as well as the geometry of the microdomain structures.

For a diblock copolymer composed of A and B blocks, the order of the blocks in the polymer chain is not important because AB and BA diblock copolymers are indistinguishable in terms of their thermodynamics and microdomain structures. However, for a triblock copolymer consisting of A, B and C blocks, the order of the three blocks arranged in the polymer chain is extremely important. Not only the primary structures of ABC, BAC and ACB triblock copolymers are distinguishable, but also their thermodynamic properties and microphase transitions are expected to be significantly different. The theoretical study predicted that attaching C block to one end of an AB diblock copolymer with a covalent bond should alter the repulsive interaction between A and B.[9] This effect may also depend on which end C block is attached to. A significant

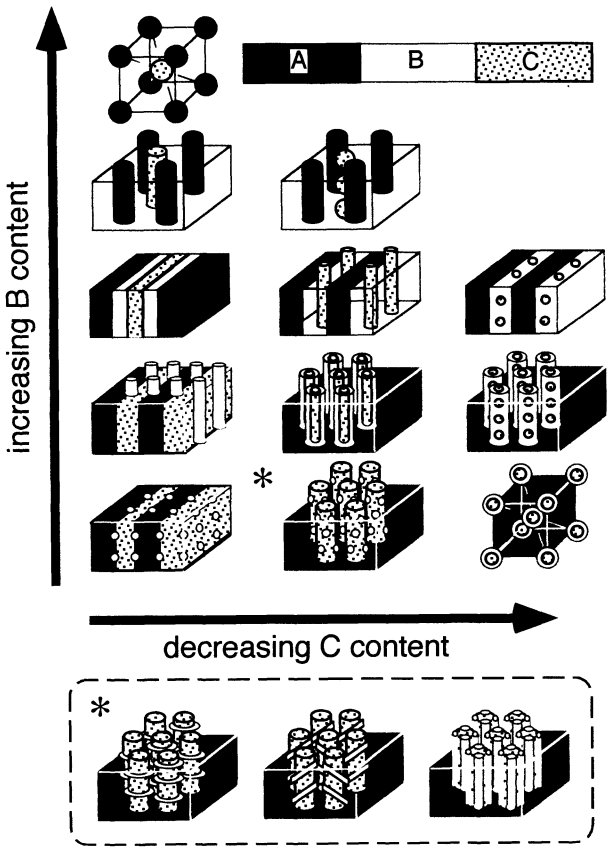

Figure 1. Possible microdomain morphologies for three-phase structures of ABC triblock copolymers composed of lamellar, cylindrical and spherical microdomains. For the composition marked by * three different models shown below can be considered depending on the relative orientation of the two kinds of cylinders.

† To whom correspondence should be addressed (e-mail: hasegawa@alloy.polym.kyoto-u.ac.jp).

change in the phase diagrams of triblock copolymers has been predicted for different sequence orders.[8]

It is obvious that the polymorphism appearing in ABC triblock copolymers is much richer compared with diblock copolymers. Just the combinations of three popular morphologies (lamellae, cylinders and spheres) result in 15 different morphologies possible for the three-phase structures of ABC triblock copolymers as illustrated in Figure 1. Although the models shown in Figure 1 are nothing but a simple geometrical prediction, some of them have been experimentally observed already.[3–6] If we take into account more complex morphologies such as the bicontinuous structures and perforated lamellae, the morphological variation will become tremendously large. In addition, an extremely complex morphology (named "knitting pattern") unpredictable from the previous knowledge was recently reported.[7] The "knitting pattern" structure analyzed by small-angle X-ray scattering (SAXS) and transmission electron microscopy (TEM) was planar with two unequal sides and exhibited the microdomain interfaces with highly non-constant mean curvature.

Such complex morphologies appearing in ABC triblock copolymers may be attributed to their complex microphase-separation processes. In general, sample specimens for structural analyses are prepared by casting from polymer solutions. In a diblock copolymer solution, the microphase separation occurs as soon as it reaches the critical concentration during the solvent evaporation process.[10] However, in an ABC triblock copolymer solution, the microphase separation consists in general of two processes: (i) one component segregates from the others, and (ii) the remaining two components segregate from each other. As a special case these two processes proceed simultaneously. Otherwise, the microphase separation proceeds in two steps The first step is analogous to the microphase separation of a diblock copolymer. The second step is the phase separation of the two components in the nano-space confined by the microdomains of the third component formed in the first step. The resulting three-phase structure is non-equilibrium one. It may eventually change to the equilibrium structure if the mobility of the system is large enough, or if not, the non-equilibrium structure may remain in bulk. A variety of microdomain structures may be produced through a variety of processes.

For an analysis of a three-phase structure, it is necessary to distinguish the three different phases. Observation of ultrathin sections by TEM along with a selective-staining technique is widely used for the investigations of three-phase structures in ABC triblock copolymers.[11] Two different staining agents, e.g., one stains A and the other stains B, may be used to distinguish the three phases. In some cases one agent stains two components with different contrast so that the three-phase structure characterized by dark, gray and bright areas can be seen. However, in many cases it is not easy to find such a staining agent. Moreover, staining is a chemical modification of polymer samples and there may be, more or less, a destructive effect on the structure. Therefore, it is desirable to establish a new TEM technique to observe the microdomain structures without staining. In this study we employed a new TEM technique, i.e., instead of using transmitted and elastically scattered electrons, we utilized inelastically scattered electrons to obtain a TEM image. Such a technique has been known for more than 10 years as element spectroscopic (or specific) imaging (ESI) or energy-filtered transmission electron microscopy (EF-TEM).[12]

We also employed SAXS for the analysis of the microdomain structure of an ABC triblock copolymer. SAXS alone is powerless to analyze such a complex structure as shown in Figure 1. However, once the structural model is determined by the real-space observation with TEM, a quantitative analysis of the structure with high precision becomes possible by SAXS. On the other hand, TEM observation is limited to the local structure. Thus, SAXS and TEM are supplementary to each other.

EXPERIMENTAL

Materials

The polymer sample used in this study was a poly(2-hydroxyethyl methacrylate)-*block*-poly(*tert*-butyl methacrylate)-*block*-poly(2-(perfluorobutyl)ethyl methacrylate) triblock copolymer (code: H-2T-F) prepared by living anionic polymerization. The synthesis procedure was reported elsewhere.[13] The characteristics of H-2T-F are summarized in Table I. A film specimen was prepared by casting from a 5 wt% solution in the 1:4 mixture (by weight) of methanol and tetrahydrofuran (THF), which is considered to be a nearly neutral solvent for all three components, H, T and F. The solution was poured into a Petri dish placed in a glass vessel and the solvent was evaporated slowly over 7 days at room temperature. The thickness of the as-cast film was ca. 0.3 mm which is thick enough for the bulk morphology to be produced in it. Ultrathin sections for TEM observations were prepared by ultramicrotoming from the as-cast film using an LKB Ultrotome Type 4801A ultramicrotome with a glass knife at room temperature. Some of the specimens were stained with 1% aqueous solution of phosphotungstic acid (PTA) after ultramicrotoming.

Table I. Characteristics of H-2T-F triblock copolymer

M_n	M_w/M_n	Composition (wt%)		
		H	T	F
6.1×10^4	1.03	23	48	29

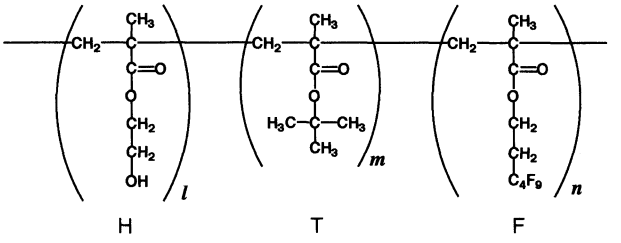

Transmission Electron Microscopy

The microdomain structure in the as-cast film of H-2T-F was observed under a transmission electron microscope by three techniques; (i) conventional transmission electron microscopy (CTEM) of stained ultrathin sections, (ii) transmission electron microscopy with element spectroscopic imaging (ESI-TEM) of unstained ultrathin sections (i.e., an image at energy loss ΔE and with energy width δE), and (iii) energy filtering transmission electron microscopy (EF-TEM) of unstained ultrathin sections. All the experiments were carried out with a JEM-2000FXZ transmission

electron microscope equipped with a GATAN imaging filter model GIF200 at an acceleration voltage of 200 keV. Element distribution images were acquired via the three-window (or three-area) method.[12] In all cases the recording time for each image was 15 sec.

SAXS

The SAXS measurements were performed with the apparatus consisting of an 18 kW rotating-anode X-ray generator (MAC Science Co. Ltd., Japan), a graphite-crystal incident-beam monochromator, and a 1.5 m camera.[14] The as-cast film specimen was set with the incident X-ray beam normal to the film surface (through configuration) and the SAXS profiles were obtained with a one-dimensional position-sensitive proportional counter (PSPC). The SAXS profile of H-2T-F was corrected for air scattering, absorption and thermal diffuse scattering (TDS) but was not corrected for slit smearing.

RESULTS AND DISCUSSION

Figure 2 shows the electron energy-loss (EEL) spectrum obtained from the ultrathin section of the as-cast film of H-2T-F. The acceleration voltage E_0 was 200 keV and a collection angle 6.79 mrad. The spectrum is characterized by the intense zero-loss peak at ΔE = 0 eV due to the electrons transmitted without suffering any measurable energy loss including those which are elastically scattered in the forward direction, and the broad plasmon peak at $\Delta E \cong 25$ eV due to the inelastic scattering as a result of the collective excitation phenomenon of the valence electrons (Figure 2a) in addition to the ionization edges of inelastic scattering resulting from the excitation of inner-shell atomic electrons (Figures 2b and 2c). Inner-shell excitation takes the form of an edge rather than a peak because the intensity rises rapidly and further decreases with increasing energy loss. The energy-loss coordinate at the sharp rise approximately corresponds to the binding energy of the atomic shell that depends on the atomic number. Thus the presence of the ionization edges indicates the kinds of elements in the sample specimen. Since the spectrum was obtained from the sample area much larger than the microdomain spacing (ca. 35 nm as shown later), it contains the ionization edges of all the elements in the sample, i.e. carbon K-edge at ΔE = 284 eV, oxygen K-edge at ΔE = 532 eV and fluorine K-edge at ΔE = 685 eV. The fluorine K-edge is clearly seen in Figures 2b and 2c (a blow-up of the square area in Figure 2b) though the intensity is very weak. All three components of H-2T-F contain carbon and oxygen atoms, but only F component uniquely contains fluorine atom. Therefore, we performed elemental mapping of fluorine atoms to determine the structure via the three-window method.[12, 15]

For the elemental mapping core-loss intensity (inelastic scattering by K-shell electrons of fluorine atoms as shown by the hatched area in Figure 2c) must be isolated by subtracting the background intensity (broken curve in Figure 2c) which can be approximated by a power-law:

$$I(\Delta E) = A\ \Delta E^{-r} \qquad (1)$$

where A and r are constants and determined by fitting Eq. (1) with the intensity data immediately preceding the edge. A series of energy-filtered images as shown in Figure 3 were obtained from the same area of the ultrathin section

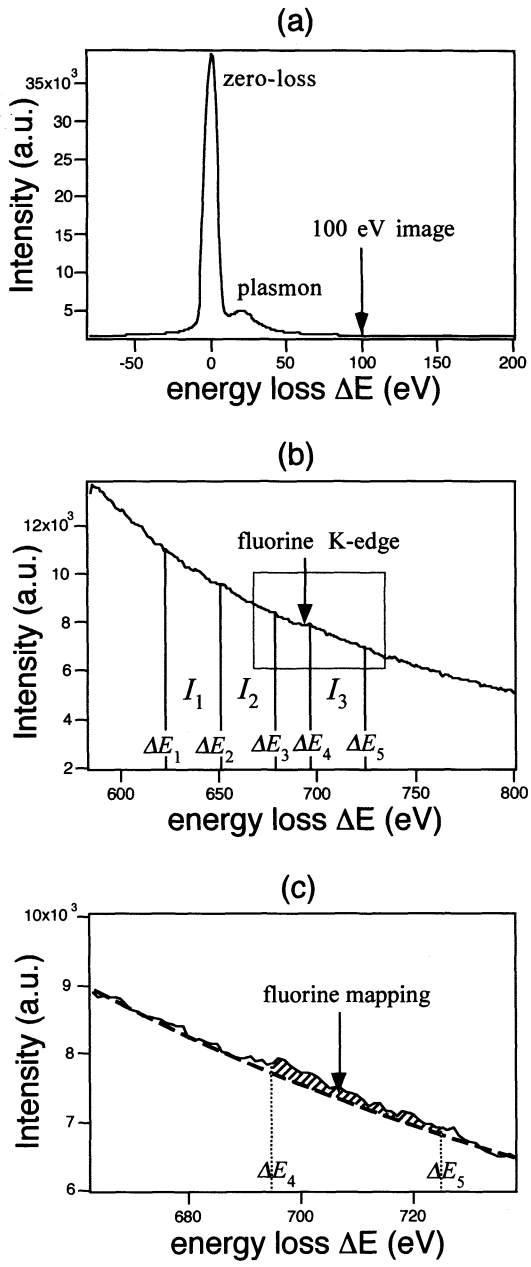

Figure 2. Electron energy-loss spectrum obtained for H-2T-F triblock copolymer. (c) is a blow-up of the area marked by a square in (b). The core-loss intensity used for the fluorine mapping is indicated by the hatched area in (c).

with a thickness of ca. 32 nm. Figure 3c was taken at ΔE = 710 eV (post-edge image of the fluorine K-edge), and Figure 3a and 3b were taken at ΔE = 637 eV and ΔE = 667 eV just preceding the fluorine K-edge (pre-edge images) with an energy width of 30 eV. The elemental mapping was done by calculating the core-loss intensity for each picture element of Figures 3a, 3b and 3c which correspond to regions $\Delta E_1 - \Delta E_2$ (intensity I_1), $\Delta E_2 - \Delta E_3$ (intensity I_2) and $\Delta E_4 - \Delta E_5$ (intensity I_3) as indicated in Figure 2b, respectively. The core-loss intensity for the mapping is given by

$$I_3 - A\ (\Delta E_5^{1-r} - \Delta E_4^{1-r}) / (1-r) \qquad (2)$$

Here, r and A are given by

$$r = 2\ \log(I_1/I_2) / \log(\Delta E_3/\Delta E_1) \qquad (3)$$

$$A = I_2(1-r) / (\Delta E_3^{1-r} - \Delta E_2^{1-r}) \qquad (4)$$

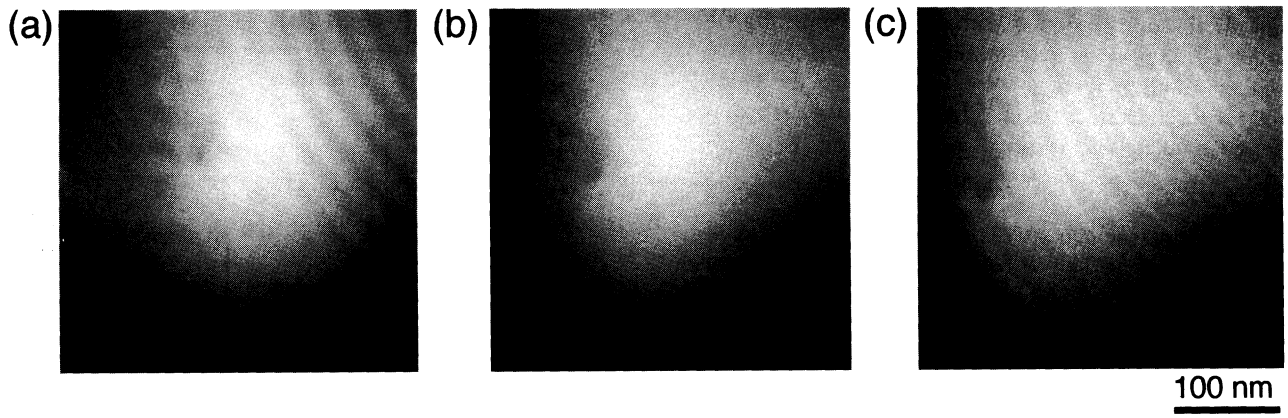

Figure 3. Energy-filtered images for H-2T-F obtained from the same area at (a) $\Delta E = 637$ eV, (b) $\Delta E = 667$ eV (pre-edge images) and (c) $\Delta E = 710$ eV (post-edge image of the fluorine K-edge) with an energy width of 30 eV.

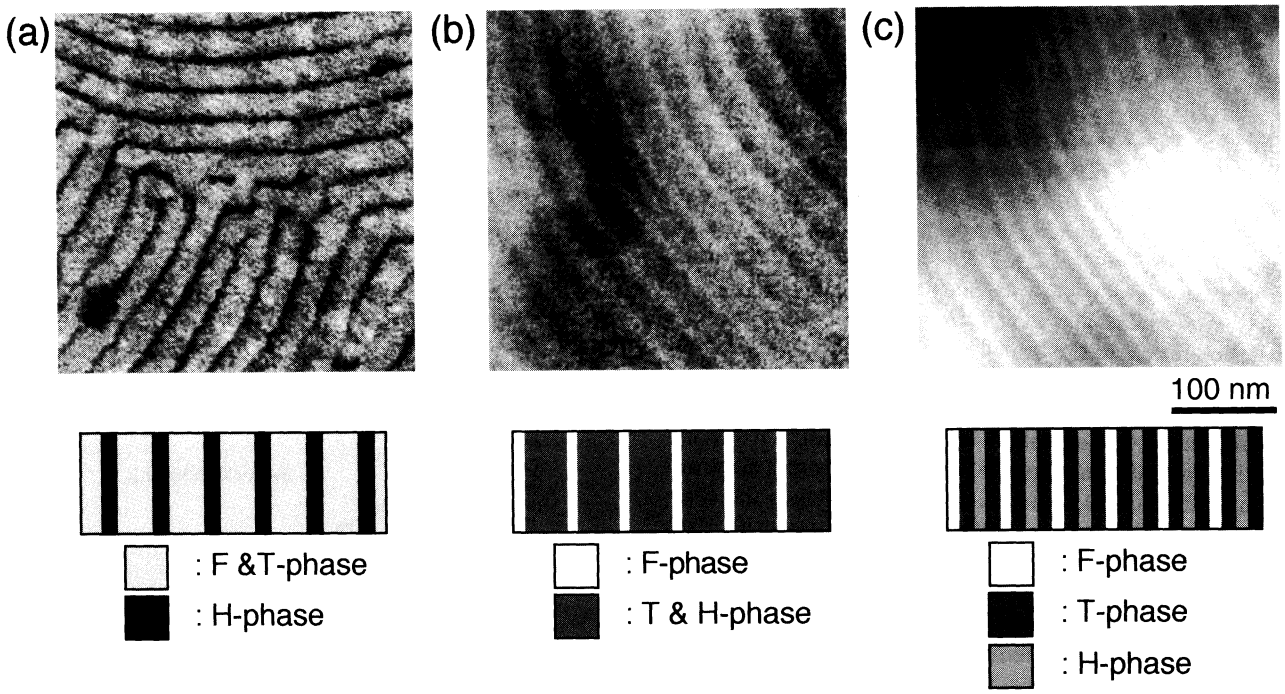

Figure 4. TEM images of H-2T-F obtained by various techniques: (a) conventional TEM image obtained with a PTA-stained specimen. (H-phase is stained dark), (b) fluorine-mapping image obtained by ESI from the EF-TEM images in Figure 3 (F-phase appears bright), and (c) EF-TEM image obtained at $\Delta E = 100$ eV with an energy width of 30 eV exhibiting the three-phase contrast. The schematic models are given below.

The resulting fluorine-mapping image of H-2T-F is shown in Figure 4b. The bright area corresponds to the region rich in fluorine atoms, i.e., the F-phase, while the H- and T-phases appear dark. The F-phase in H-2T-F seems to form lamellar microdomains as schematically illustrated below in Figure 4b. Figure 4a shows a CTEM image of a PTA-stained ultrathin section prepared separately. The dark regions correspond to the H-phase selectively stained by PTA, while the unstained F- and T-phases appear bright. The H-phase also seems to form lamellar microdomains. The spacing of the dark lamellae (H-phase) in Figure 4a and that of the bright lamellae (F-phase) in Figure 4b are both ca. 35 nm. These observations and the consideration of the block sequence of H-2T-F immediately lead to a four-layered lamellar structure with the repeat unit of H–T–F–T.

Figure 4c is a energy-filtered image obtained from the same area as shown in Figure 3 and Figure 4b but was taken at $\Delta E = 100$ eV with an energy width of 30 eV. Surprisingly, the four-layered lamellar structure is clearly seen with a good contrast of three levels, i.e., dark, gray and bright as schematically shown below in the figure. The bright area exactly matches the bright area in Figure 4b corresponding to the F-phase. Then, the gray and dark areas correspond to H- and T-phases, respectively. The thickness of H, T and F microdomains is ca. 10, 8 and 9 nm, respectively.

Since inner-shell ionization edges occur mostly at energy-losses above 100 eV, the scattering at $\Delta E = 100$ eV consists of the monotonically decreasing background scattering which originates from the excitation of atomic electrons of lower binding energy. Therefore, the contrast should be able to be explained by the inelastic scattering from the atomic electrons of lower binding energy. However, strict evaluation of the inelastic scattering intensity of each phase is not practical because of the uncertainty involved in the experiment. So we roughly estimated the relative intensity of the three phases based on the elemental composition and density of each phase. As for the density

of each phase we used the bulk density measured for the corresponding homopolymers (1.168 and 1.892 g/cm^3 for T and F homopolymers, respectively). The density of H phase (1.347 g/cm^3) was estimated from the value of k_1/k_2, the ratio of electron density differences between F- and T-phases and between H- and T-phases, obtained in the SAXS analysis described later, because the accurate measurement of the density of H homopolymer was difficult due to its moisture absorption. (But the measurement suggested that the density of H homopolymer was located between those of T and F homopolymers.) Contribution of hydrogen atoms to the scattering intensity may be ignored because the radiation damage quickly eliminates them from the specimen. If we use the ratio of atomic total inelastic cross section 2.6:1.7:1.3 for carbon:oxygen:fluorine (calculated by Inokuti et al.[16] for 80 keV electrons), the ratio of inelastic scattering intensity for F-, H- and T-phase becomes 23:21:20, which agrees with our observation in Figure 4c. This order does not alter even if we assume that total inelastic cross sections of all atoms are equal. Although H- and T-phases contain only common elements such as hydrogen, carbon and oxygen, they showed a clear contrast. This suggests that EF-TEM may give a good contrast for block copolymers such as polystyrene-*block*-polyisoprene and polymer blends even if the component polymers do not contain a unique element. Differences in elemental composition and density of the two phases determine the contrast. Thus, EF-TEM may open a great possibility for the structural study of multiphase polymer systems.

Although EF-TEM is powerful to determine the morphological model of a microdomain structure, the statistics for the quantitative analysis is not satisfactory. On the other hand, it is not easy to identify the morphology by SAXS when the morphological variation is so large as a part of it is shown in Figure 1. Nevertheless, SAXS can provide the quantitative information on a structure of nm scale. A very precise structural analysis is possible with SAXS when it is combined with EF-TEM. Therefore, we performed SAXS measurements of the as-cast film of H-2T-F. The SAXS profile of H-2T-F after corrections for air scattering, absorption and thermal diffuse scattering is shown by the data points in Figure 5a. The profile is characterized by many peaks, the higher-order peaks of which appear at the momentum transfer q of an integer multiples of that of the first-order peak suggesting a layered structure. The scattering profile has a peculiar feature, i.e., the intensity of the second-order peak is higher than that of the first-order peak, which has never been reported for a diblock copolymer. However, it is possible to calculate the SAXS intensity distribution since the morphology is already known by the EF-TEM result.

We employed a one-dimensional paracrystal analysis technique.[17,18] Figure 6 shows the spatial distribution of the electron density along the lamellar normal based on the four-layer model of H–T–F–T sequence. With this model the form factor f^2 of the one-dimensional particle is given by

$$f^2 = \iint \left\{ k_1 \frac{\sin(qx/2)}{(qx/2)} \exp\left(\frac{-\sigma^2 q^2}{2}\right) - k_2 \frac{\sin(qy/2)}{(qy/2)} \exp\left(\frac{-\sigma^2 q^2}{2}\right) \right\}^2 \exp\left\{ -\left[x - (d_1 + 2d_2)\right]^2 / 2\sigma_x^2 \right\} \exp\left[-(y - d_1)^2 / 2\sigma_y^2 \right] dy dx \quad (5)$$

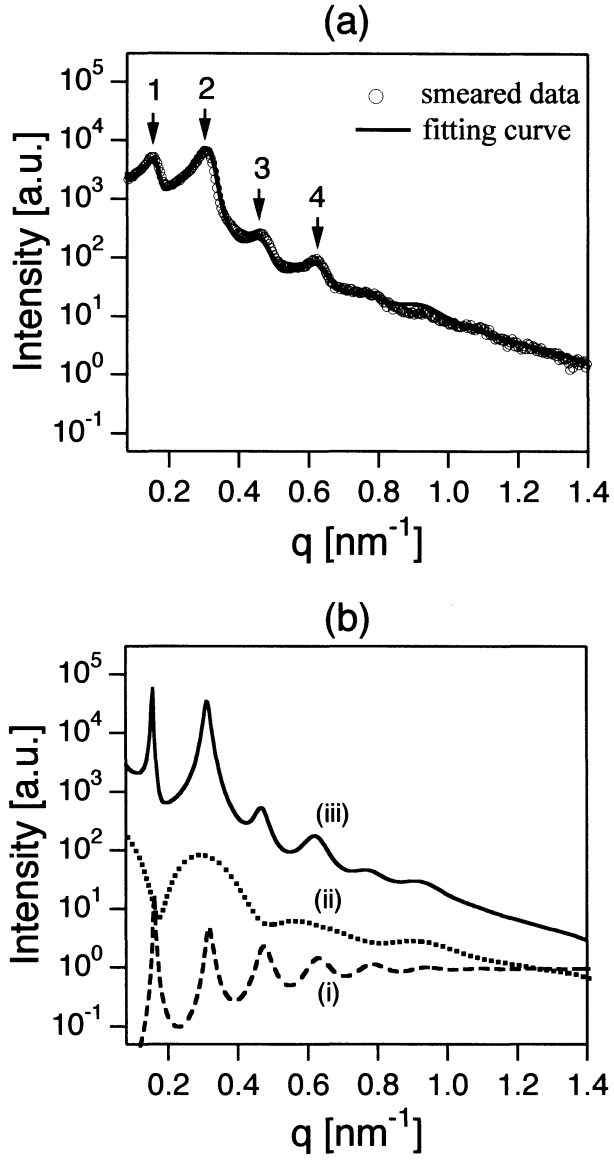

Figure 5. (a) SAXS profile obtained for H-2T-F (data points) and the smeared theoretical curve best fitted to the data (solid curve). (b) Calculated curves for the lattice factor Z (curve i), form factor f^2 (curve ii) and scattering intensity $I(q)$ (curve iii) with the best-fitted parameters for H-2T-F.

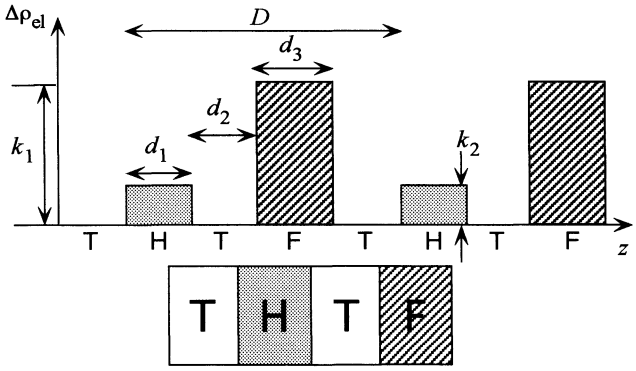

Figure 6. One-dimensional electron-density distribution model for the paracrystal analysis of the four-layer structure of H-2T-F.

where d_1 and d_2 are the thickness of H and T lamellar phases and k_1 and k_2 are the electron density differences ($\Delta\rho_{el}$) between F- and T-phases and H- and T-phases, respectively. σ is related to the interfacial thickness t by the relation, t =

$(2\pi)^{1/2}\sigma$. The integration interval is $0–2d_1$ for y and $0–2(d_1+2d_2)$ for x. σ_x and σ_y introduce gaussian distributions to the layer thickness. The lattice factor Z for the one-dimensional lattice with spacing D ($= d_1+2d_2+d_3$) is given by

$$Z = (1-|F|^2) / (1-2|F|^2\cos(qD)+ |F|^2) \quad (6)$$

$$|F| = \exp(-g^2D^2q^2 / 2) \quad (7)$$

where g is Hosemann's g parameter defined as $g \equiv \sigma_D/D$ (σ_D is the standard deviation of D assuming a gaussian distribution of D). Then, the scattering intensity for the partially oriented or randomly oriented lamella system $I(q)$ is given by

$$I(q) \sim q^{-2}f^2Z \quad (8)$$

Furthermore, theoretical scattering intensity $I(q)$ was smeared with the slit-width and slit-height weighting functions, $W(Q_x)$ and $W(Q_y)$, respectively, which were determined for the SAXS optics used in this work, and the smeared intensity $I_s(q)$ calculated by the equation

$$I_s(q) \sim \int_{-\infty}^{\infty}\int_{-\infty}^{\infty} W(Q_x)W(Q_y)I(q)\left[(q-Q_x)^2 - Q_y^2\right]^{1/2} dQ_x dQ \quad (9)$$

was compared with the experimental scattering profile in Figure 5a. In Figure 5b, (i) Z, (ii) f^2 and (iii) $I(q)$ for the best-fitted case are shown. It should be noted that the first minimum of f^2 occurs at q close to the first-order peak of Z. This considerably reduces the intensity of the first-order peak relative to that of the second-order peak in $I(q)$. In some cases, the second-order peak can be more intense than the first-order peak. However, in the particular case of H-2T-F, the first-order peak of $I(q)$ is still higher than the second-order one. Therefore, it is a smearing effect that causes the inversion of the intensity as shown in Figure 5a. The smeared theoretical scattering curve $I_s(q)$ (solid curve in Figure 5a) matches the data points very well.

Finally, the parameters obtained by the SAXS paracrystal analysis as well as the data obtained by the EF-TEM observation were listed in Table II. The average repeat distance D and the average thickness of H-, T- and F-phases d_1, d_2 and d_3, respectively, show a good agreement, taking into account the experimental errors in the TEM observations. The electron density estimated from the bulk density data is 3.858 and 5.694 $\times 10^{23}$ electron/cm^3 for T- and F-phase, respectively. The electron density of H-phase estimated from the ratio of k_1/k_2 is 4.363 $\times 10^{23}$ electron/cm^3 and hence the density becomes 1.347 g/ cm^3.

CONCLUSION

EF-TEM and ESI were proved to be extremely useful for morphological investigations of block copolymers especially by giving different contrast to each phase of ABC triblock copolymers without any staining. A peculiar SAXS profile in which the first-order peaks have lower intensity than the second-order was observed for H-2T-F triblock copolymer. The SAXS paracrystal analysis with the four-layer lamella model based on the EF-TEM observation successfully reproduced the unusual SAXS profile.

Table II. Structural parameters obtained by SAXS paracrystal analysis and EF-TEM observation

	SAXS	EF-TEM
k_1	2.0	
k_2	0.55	
d_1 (nm)	11	10
d_2 (nm)	9.5	8
d_3 (nm)	10	9
D (nm)	40	35
g	0.07	
t (nm)	1.5	

Acknowledgment. The authors gratefully acknowledge the partial financial supports of a Grant-in-Aid for Scientific Research (10126230) from the Ministry of Education, Science, Sports and Culture of Japan.

REFERENCES

1. H. Hasegawa, H. Tanaka, K. Yamasaki, and T. Hashimoto, *Macromolecules*, **20**, 1651 (1987).
2. F. S. Bates, M. F. Schulz, A. K. Khandpur, S. Förster, J. H. Rosedale, K. Almdal and K. Mortensen, *Faraday Discussi.*, **98**, 7 (1994).
3. G. Riess, M. Schlienger, and S. Marti, *J. Macromol. Sci., PolymPhys.Ed.*, **B17**, 355 (1980).
4. I. Kudose and T. Kotaka, *Maclomolecules*, **17**, 2325 (1984).
5. Y. Mogi, H. Kotsuji, Y. Kaneko, K. Mori, Y. Matsushita, and I. Noda, *Macromolecules*, **25**, 5408 (1992).
6. R. Stadler, C. Auschra, J. Beckmann, U. Krappe, I. Voigt-Martin, and L. Leibler, *Macromolecules*, **28**, 3080 (1995).
7. U. Breiner, U. Krappe, E. L. Thomas, and R. Stadler, *Macromolecules*, **31**, 135 (1998).
8. W. Zeng and Z.-G. Wang, *Macromolecules*, **28**, 7215 (1995).
9. I. Erukhimovich, V. Abetz, and R. Stadler, *Macromolecules*, **30**, 7435 (1997).
10. M. Shibayama, T. Hashimoto, H. Hasegawa, and H. Kawai, *Macromolecules*, **16**, 1427 (1983).
11. M. Shibayama, T. Hashimoto, H. Hasegawa, and H. Kawai, *Macromolecules*, **15**, 274 (1982).
12. R. F Egerton, "Electron Energy-Los Spectroscopy in the Electron Microscope, 2nd Ed.," Plenum Press, New York, N.Y., 1996.
13. T. Ishizone, K. Sugiyama, Y. Sakano, H. Mori, A. Hirao, and S. Nakahama, *Polym. J.*, in press.
14. T. Hashimoto, S. Suehiro, M. Shibayama, K. Saijo and H. Kawai, *Polym. J.*, **13**, 501 (1981).
15. M. Kawasaki, T. Oikawa, K. Ibe, K. Park, M. Shiojiri, *J. Electron Microsc.*, **47**, 477 (1998).
16. M. Inokuti, R. P. Saxon, and J. L. Dehmer, *Int. J. Radiat. Phys. Chem.*, **7**, 109 (1975).
17. M. Shibayama and T. Hashimoto, *Macromolecules*, **19**, 740 (1986).
18. S. Koizumi, H. Hasegawa, and T. Hashimoto, *Macromolecules*, **27**, 7893 (1994).